crystals

MDPI

Review

Dislocation Motion and the Microphysics of Flash Heating and Weakening of Faults during Earthquakes

Elena Spagnuolo [1,*], Oliver Plümper [2], Marie Violay [3], Andrea Cavallo [1] and Giulio Di Toro [1,4,5]

1 Sezione di Sismologia e Tettonofisica, Istituto Nazionale di Geofisica e Vulcanologia, Via di Vigna Murata 605, 00143 Roma, Italy; andrea.cavallo68@gmail.com (A.C.); giulio.ditoro@manchester.ac.uk (G.D.T.)
2 Department of Earth Sciences, Utrecht University, Budapestlaan 4, 3584 CD Utrecht, The Netherlands; O.Plumper@uu.nl
3 LEMR, ENAC, École polytechnique fédérale de Lausanne (EPFL), 1015 Lausanne, Switzerland; marie.violay@epfl.ch
4 Dipartimento di Geoscienze, Università di Padova, Via G. Gradenigo 6, 35131 Padova, Italy
5 School of Earth, Atmospheric and Environmental Sciences, Manchester University, Oxford Street, M13 9PL Manchester, UK
* Correspondence: elena.spagnuolo@ingv.it; Tel.: +39-06-51860729

Academic Editor: Ronald W. Armstrong
Received: 5 July 2016; Accepted: 16 July 2016; Published: 22 July 2016

Abstract: Earthquakes are the result of slip along faults and are due to the decrease of rock frictional strength (dynamic weakening) with increasing slip and slip rate. Friction experiments simulating the abrupt accelerations (>>10 m/s^2), slip rates (~1 m/s), and normal stresses (>>10 MPa) expected at the passage of the earthquake rupture along the front of fault patches, measured large fault dynamic weakening for slip rates larger than a critical velocity of 0.01–0.1 m/s. The dynamic weakening corresponds to a decrease of the friction coefficient (defined as the ratio of shear stress vs. normal stress) up to 40%–50% after few millimetres of slip (flash weakening), almost independently of rock type. The microstructural evolution of the sliding interfaces with slip may yield hints on the microphysical processes responsible for flash weakening. At the microscopic scale, the frictional strength results from the interaction of micro- to nano-scale surface irregularities (asperities) which deform during fault sliding. During flash weakening, the visco-plastic and brittle work on the asperities results in abrupt frictional heating (flash heating) and grain size reduction associated with mechano-chemical reactions (e.g., decarbonation in CO_2-bearing minerals such as calcite and dolomite; dehydration in water-bearing minerals such as clays, serpentine, etc.) and phase transitions (e.g., flash melting in silicate-bearing rocks). However, flash weakening is also associated with grain size reduction down to the nanoscale. Using focused ion beam scanning and transmission electron microscopy, we studied the micro-physical mechanisms associated with flash heating and nanograin formation in carbonate-bearing fault rocks. Experiments were conducted on pre-cut Carrara marble (99.9% calcite) cylinders using a rotary shear apparatus at conditions relevant to seismic rupture propagation. Flash heating and weakening in calcite-bearing rocks is associated with a shock-like stress release due to the migration of fast-moving dislocations and the conversion of their kinetic energy into heat. From a review of the current natural and experimental observations we speculate that this mechanism tested for calcite-bearing rocks, is a general mechanism operating during flash weakening (e.g., also precursory to flash melting in the case of silicate-bearing rocks) for all fault rock types undergoing fast slip acceleration due to the passage of the seismic rupture front.

Keywords: earthquake mechanics; high speed rock deformation; dislocations; weakening mechanisms; calcite

1. Introduction

During an earthquake, at any distance away from the nucleation area, the passage of the rupture front at a few km/s results in abrupt accelerations and fault slip reaching speeds up to several m/s within a few milliseconds [1]. The seismic rupture propagates because the local friction coefficient (μ, ratio of shear stress τ with normal stress σ_n) of the fault decreases from typical Byerlee's values ($\mu \sim 0.70$) down to 0.05 with increasing slip and slip rates upon the activation of a series of weakening mechanism [2,3]. In the last 20 years, the advent of the so called high-speed rotary shear machines, allowed us to reproduce deformation conditions that approach those achieved at the rupture front during seismic slip [4]. From these experiments it became clear that more or less independently of the lithology, fault rocks undergo profound weakening when a critical slip rate V_w of 0.01–0.1 m/s is exceeded [2,5,6].

So far, the connection between slip rate and weakening has been studied in relation to the frictional heat production at the asperity scale. Theoretical and experimental investigations [5,7–15] on silicate-bearing rocks (gabbro, granite, peridotite, etc.) suggested that such frictional heat initiates at highly stressed microscopic asperities, a process termed flash heating. When the velocity is such that the contact time of the rubbing asperities is large compared to the time it takes for heat to diffuse away from the asperities, the temperature can rise considerably resulting in instantaneous asperity melting [16]. The entire process is defined as flash heating and melting and results in dramatic weakening of the friction coefficient (>40%) after less than 1 mm of slip. With further slip, the entire fault surface is completely molten [8,14,15].

Flash weakening was also observed in other rock types, including carbonate-bearing rocks (calcitic marbles, limestones) which are not prone to melting [17–20]. After flash weakening, progressive seismic slip triggered decarbonation reactions, CO_2 emission and, possibly, the activation of grain size dependent and crystal plastic processes [18,21–24]. In the case of quartz-rich rocks, especially under wet conditions and low normal stresses (<5 MPa), weakening at the seismic slip was associated with the production of lubricating silica gels [25,26]. Importantly, in natural fault zones high temperature fault products like glasses and quenched melts (called pseudotachylites in the geological literature [27–29]), vesiculated and recrystallized calcite grains (possibly associated with decarbonation reactions [30–32]), and silica-gels were found [33]. However, experiments have also shown that the temperature itself is not the unique cause for fault weakening. Rocks sheared at sub-seismic sliding velocities (<<1 mm/s) but temperatures spanning the entire range typical of frictionally generated temperatures (bulk estimates up to 1200 °C) typically had relatively large Byerlee's friction coefficient values (μ = 0.6) (e.g., [34]). Moreover, observations on natural and experimental faults reported grain size reduction up to the nanoscale (i.e., [35–37]) and solid state amorphization [38] which could not solely be explained by an increase in temperature. As a consequence, there must be a relation between temperature rise, grain size reduction, and slip-rate having profound implications for the mechanics of earthquakes. While temperature rise and grain size reduction may explain the triggering of mineral decomposition reactions and phase changes, the relationships between slip-rate, intense grain fragmentation, temperature rise, and flash weakening are still poorly understood. Insights may come from the hypothesis that temperature increase is a macroscopic quantity resulting from the radiation emanated by the rock volume due to electronic vibrations and nano- to micro-scale deformation mediated by dislocations and crystal defects.

Lattice defects such as linear defect (dislocations) as well as microcracks and grain boundaries have been previously studied in association with earthquake microphysics [39,40] and are responsible for reduced rock strength well below the theoretical strength of crystalline materials [41]. Dislocations moving at velocities as fast as earthquake deformation rates can be responsible for flash heating and frictional strength reduction as depicted by theoretical models for shock impacts, high-speed friction [42] and recent high-speed experiments on fault rocks [20].

The study presented here is based on recent experimental results on high-speed friction experiments on carbonate-bearing rocks to build general constraints on the mechanics of fault flash weakening [20].

2. High Speed Friction Experiments in Rock Materials

The experiments discussed here were performed using SHIVA (Slow to High Velocity Apparatus, [43] HP-HT laboratory of the INGV of Rome, Italy), a high velocity rotary shear machine designed to simulate natural seismic deformation conditions in the uppermost Earth' crust (e.g., slip rates of 1 m/s and normal stress of 10 MPa). We selected Carrara marble (s769, 99% calcite) as representative of the 20% of sedimentary carbonate-bearing rocks where intra-plate earthquakes occur. Serpentinite (s735, 90% antigorite with minor magnesite and magnetite [12]) a quite common hydrated silicate-bearing mantle rock. Microgabbro (s699, plagioclase 35%–45%, clinopyroxene 25%–35%, feldspathoids 10% and titanomagnetite 5%–15%), a common silicate-bearing rock ([13,14]) which constitutes most of the lower oceanic and part of the continental crust. For all experiments (Figure 1), we used pre-cut hollow rock cylinders with an external and internal diameter of 50 and 30 mm, respectively. The cylinders were sheared under a constant normal stress (10 MPa) and room humidity conditions by imposing a trapezoidal velocity function with an acceleration and deceleration ramp of 6.5 to 65 m/s^2. All the experiments in Figure 1 show (1) an initial stage of strengthening until the achievement of an ultimate and reproducible peak in shear stress (which equals the peak in friction coefficient of 0.8 for serpentinite, 0.7 for micrograbbro, 0.65 for Carrara marble for a constant normal load) followed by (2) a pronounced weakening (~40%) after only 5 mm of slip. Independently of rock lithology, the three rock types showed a pronounced weakening at V_w ~ 0.1 m/s.

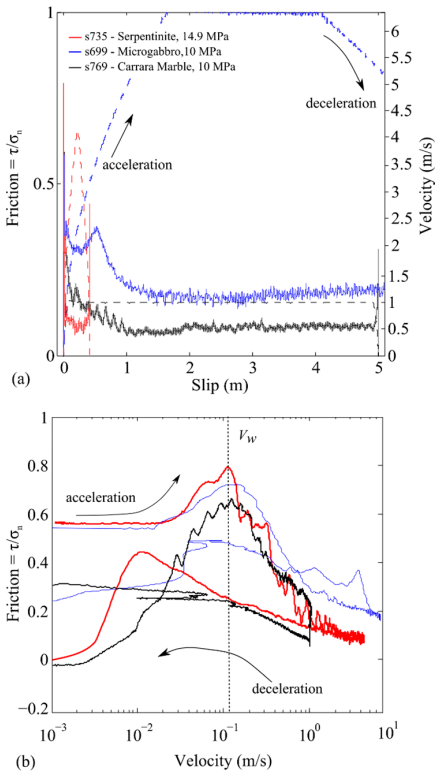

Figure 1. Frictional evolution of rocks in high velocity experiments simulating the passage of the rupture front at point of a fault during an earthquake. The experiments were performed with the rotary shear machine SHIVA. Samples were sheared at ambient conditions under a constant normal stress of σ_n = 10 MPa and at seismic slip rates (>1 m/s). (**a**) Friction coefficient evolution with slip of cohesive Carrara marble (99.9% calcite, s769), microgabbro (main mineral plagioclase, s699), and serpentinite (main mineral antigorite, s735) resulting from high-velocity friction experiments. The slip rate of the applied velocity ramp (dashed lines) is on the right y-axis; (**b**) Friction evolution with slip rate for the same experiments reported in Figure 1a. The critical velocity V_w at the onset of the large dynamic weakening was 0.103 ± 0.03 m/s.

In the case of Carrara marble, coeval to the weakening, a substantial release of CO_2 (8% increase with respect to the atmospheric concentration) was measured with a quadrupole mass spectrometer after the sample was slid for 1.5 mm and 5 mm. The Carrara marble samples from experiments stopped after 1.5 mm, 5 mm and 50 mm of slip were recovered for microstructural analysis [20]. Microstructural investigations conducted with a scanning electron microscope (SEM) and transmission electron microscope (TEM) on and just beneath the slip surface of the aforementioned samples (Figure 2), suggest an intimate correlation between the evolution of the rock's microstructure and the fault weakening. TEM images (Figure 2a) of electron-transparent focused ion beam (FIB) SEM foils of the experimental fault just beneath the slip surface at 1.5 mm of slip revealed dislocations patterns similar to those in minerals recovered from impact craters that underwent shock metamorphism (Figure 2b, [44]). Inter-cleavage crystal domains exhibit intense mosaicism, alternating between areas that are nearly dislocation free to those that exhibit a high dislocation density. Micro-fractures are closely spaced (200 nm apart). Selected area electron diffraction (SAED, inset in Figure 2b) indicates that high dislocation density areas are polycrystalline, i.e., formed by individual nanograins. Nanograins have a grain size of 5–100 nm and are dislocation free (Figure 2c). Relevant to this analysis is the evidence of decarbonation reactions (CO_2 detected by mass spectrometry: 8% after 5 mm of slip, 16% after 50 mm of slip) and the deposition of amorphous carbon (Figure 2d). Amorphous carbon was identified by energy dispersive X-ray spectroscopy both in the porous network just beneath and especially on the slip surface after 5 mm of slip (P1 in Figure 2d) but also after only 1.5 mm of slip (see [20] for details). The deposition of amorphous carbon is associated with the breakdown of CO_2 released by the calcite grains due to thermal decomposition, analogous to observed reactions occurring in the Earth interior under high pressures (more than 30 GPa) and temperature (more than 1500 °C) conditions, respectively [45].

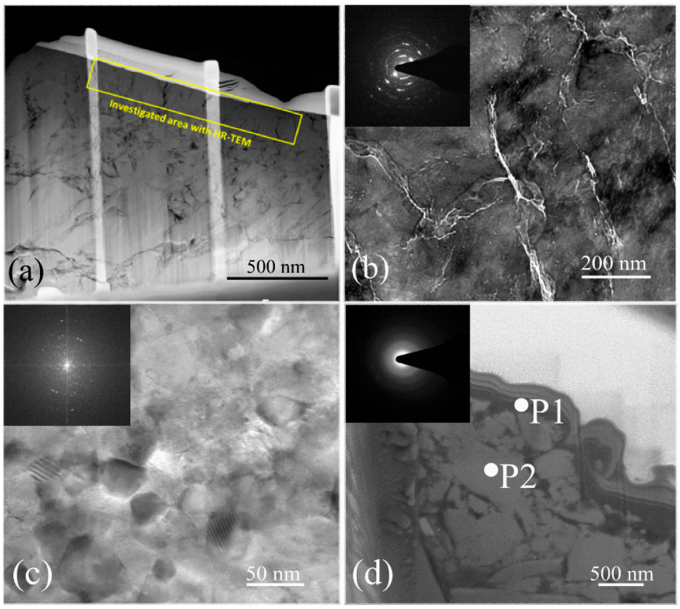

Figure 2. Microstructural investigation of deformed cohesive Carrara marble samples. (**a**) Rock volumes immediately below slip surfaces after 1.5 (**a**–**c**) mm and 5 mm of displacement (**d**). All images are from FIB-SEM specimens cut perpendicular to the slip surface and perpendicular (**a**–**c**) and parallel (**d**) to the slip direction. The slip surface is on top, coated with Platinum. (**b**) Inter-cleavage crystal domains exhibit complex TEM diffraction contrast due to a high density of crystal defects, i.e., dislocations. High density of dislocations domains remain either crystallographically coherent or develop a polycrystalline (see SAED pattern) mosaicism nanostructure. (**c**) Numerous nanograins develop within the fracture volumes (bright-field TEM images); (**c**) Deposition of amorphous carbon at 5 mm of slip. P1 is amorphous Carbon from TEM-EDS analyses. P2 is calcite.

3. The Macroscopic Flash Heating Model

The flash heating model predicts that in silicate-bearing rocks, the critical velocity V_w is related to the size (~diameter) of the contact asperities d, the melting temperature Tw, and the contact shear strength τ_c [2,46]:

$$V_w = \left(\frac{\pi \alpha_{th}}{d}\right)\left[\frac{\rho C_p \left(T_w - T_f\right)}{\tau_c}\right]^2 \quad (1)$$

where T_f is the ambient temperature, α_{th} the thermal diffusivity, ρ the rock density, and C_p the specific heat capacity (Table 1).

Table 1. Thermal and physical properties from Schön [47] with M: Melnikov et al. [48], C: Cermak and Rybach, [49]; B: Broz et al. [50]; Be = Beeler [9]. K: Koholi et al. [51].

Thermal and Physical Parameters	Calcite	Antigorite	Plagioclase
α_{th} (m^2/s)*10^{-6}	1.5–1.74	1–1.75	0.9
C_p ($kJ \cdot kg^{-1} \cdot K^{-1}$)	0.8–0.83 (M)	0.65 (M)	1.01 (C)
ρ ($kg \cdot m^{-3}$)*10^3	2.7	2.54	2.95
Λ ($Wm^{-1} \cdot K^{-1}$)	3.25–3.9 (M)	1.8–2.9 (M)	2.63 (C)
G (GPa)	35	40	34
H (GPa)	2.21 (B)	4 (K)	6.24 (Be)
b (nm)	0.49	0.53	0.5 (diopside)
Grain size	Fine grained, average 100 μm	Very Fined Grained, average 10 μm	Coarse grained, average 3 mm

Given the thermal parameters presented in Table 1, for d = 10 μm and a minimum and maximum value for τ_c (GPa) estimated as τ_c = 0.5 H (indentation hardness) and τ_c = 0.1 G (shear modulus) respectively [52], it is possible to determine from Equation (1) a range of temperatures associated with V_w (Figure 3). The diagram reports—as red dashed lines—the temperature of 800 °C for breakdown of calcite ($CaCO_3 \rightarrow CaO + CO_2$, calcite being the main constituent of Carrara marble), of 1200 °C for melting of plagioclase (main constituent of microgabbro, but clinopyroxene has a quite similar melting temperature), of 500 °C for breakdown of antigorite (dehydration reaction to talc and olivine: $Mg_3Si_2O_5(OH)_4 \rightarrow Mg_3Si_4O_{10}(OH)_2 + Mg_2SiO_4 + H_2O$, antigorite being the main constituent of the serpentinite).

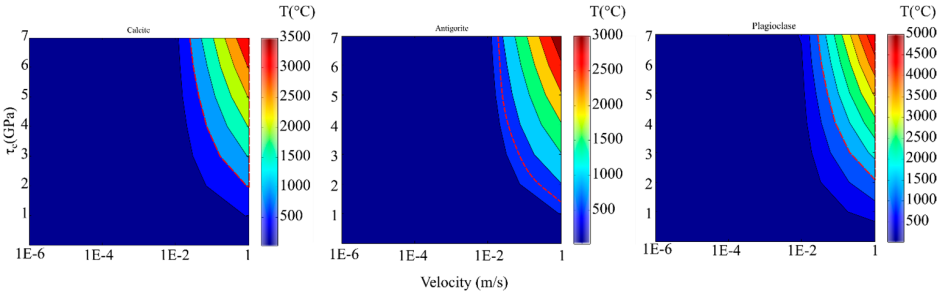

Figure 3. Temperature estimation at the asperities as a function of the ultimate shear strength and velocity resulting from the flash heating model (Equation (1)) using the thermal parameters in Table 1. From left to right, case for calcite (most abundant mineral in Carrara marble), antigorite (most abundant mineral in the tested serpentinite), and plagioclase (most abundant mineral in microgabbro).

The results of the numerical simulation in Figure 3 are consistent with weakening at V_w greater than few cm/s where the temperatures at the asperity contacts reach the conditions for the triggering of chemical reactions and phase transitions for the three lithologies examined here. Decomposition reactions (e.g., formation of amorphous carbon) and phase transitions (e.g., melting)

may contribute to lubrication at the asperity scale. The dependency of V_w on material properties, e.g., the contact stress (also of the newly formed minerals), and on microstructural characteristics, e.g., the grain size, show the relevance of mechano-chemical reactions in fault weakening.

4. Moving Dislocations at the Ductile-Brittle Transition

The deformation of crystalline solids is often accommodated by the movement of dislocations and creation of new ones. The concept of dislocations in a solid was first mechanistic connected to plasticity in the early 1930s to explain the ease of solids to flow with respect to theoretical predictions, i.e., [53]. The nature and theory of dislocations and their connection to Earth materials is well discussed in a number of previous works [41,54–56]. Under an applied stress, pre-existing or newly formed dislocations move inside the crystal lattice until encountering an obstacle. When the obstacle is a grain boundary, a large atomic mismatch opposes a stress field to dislocation motion. This repulsive stress, including phonon scattering, impurity drag, and lattice periodicity (e.g., the Peierls potential) acts as an energetic barrier. The energy barrier can be overcome by thermal fluctuations, or when a number of dislocations pile-up to generate a collective repulsive stress field (e.g., [57]). The rate at which obstacles are overcome by thermal fluctuations depends on the vibration frequency of a dislocation f_d, which in turn depends on the length of the dislocation. Thus, the strength of the material and its viscous-plastic flow depends on how easily dislocations are formed and destroyed, on the amount of energy required to move them in the lattice, and on the time needed to overcome the energy barrier by thermal fluctuations.

As the strain rate increases, there is less time available for the moving dislocations to overcome the energetic barrier until, above a critical strain rate $\dot{\gamma}^*$, thermal activation is rendered ineffective. At high strain rates stress relaxation—occurring by the collective motion of discrete newly formed or pre-existing dislocations—is inhibited and an effective applied stress equal to the full obstacle strength has to be provided to overcome the obstacle [58,59]. As a consequence, dislocations pile-up in arrays distributed along the microstructural obstacle, as schematized in Figure 4a, where the stress increases until it reaches the yield point (see also Section 7). The onset of brittle failure (and dynamic weakening) occurs when the stress is instantaneously released resulting in catastrophic dislocation avalanches (Figure 4b, [60,61]). These avalanches result in an ultrafast dissipation of dislocation kinetic energy into heat for generation of so-called "hot-spots", the emission of newly formed dislocations and fast stress release [58–62]. The ductile failure behavior typical of low strain rates turns into a brittle failure under highly dynamic conditions [63].

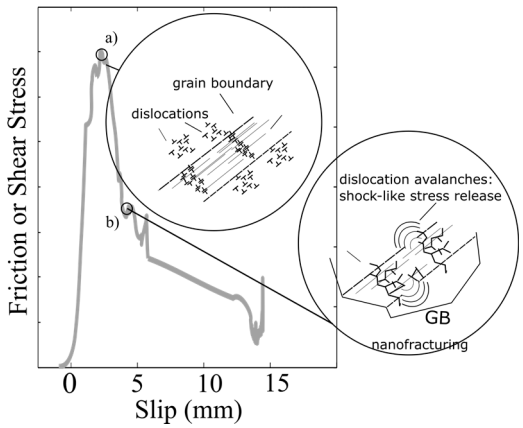

Figure 4. Evolution of microstructures and shear stress with slip. At slip initiation (panel **a**), the asperities are strained: new dislocations are emitted and pile up at microstructural obstacles (e.g., cleavage planes, grain boundaries). With progressive slip (and strain, panel **b**) the stress exerted by the piled-up dislocations overcomes the yield strength of the obstacle and the dislocations are released in "avalanches" causing brittle failure, formation of nano-grains, and temperature increase (flash heating) [20].

5. Fast-Moving Dislocations Trigger Flash Heating in Fault Rocks

The consequence of fast dislocation motion is to separate highly compressed from uncompressed regions inducing grain fragmentation and mosaicism within the lattice as observed in Carrara marble (Figure 2b) and in the case of impact structures [44]. The separation between physical parameters in front and behind the so called shock-front represents a violent discontinuity in all state parameters like temperature, density, pressure, and internal energy [64,65], which is accomplished by an instantaneous reorganization of the internal strain. Moreover, a vast amount of kinetic motion is dissipated into heat from dislocation avalanches in an extremely narrow (~20–30 Burgers vectors in thickness, [57]) shear zone and in a time shorter than 100 ms. The extreme localization and the short time causes a large and adiabatic (the heat is produced faster than it is conducted away via diffusion) temperature increase (several hundred °C) at the asperity contacts. The abrupt temperature rise leads to decarbonation reactions and deposition of amorphous carbon in the case of the experiments performed on Carrara marble (Figure 2d, see also [20]).

The fast-moving dislocation model thus explains a number of experimental observations occurring at the onset of dynamic weakening in particular the abrupt temperature increase leading to decarbonation reactions in calcite-bearing rocks for instance, phase transformations in silicate-bearing rocks (possibly melting), but also the grain size reduction to the nanoscale [20]. Moreover, as discussed below, given the existence of a strain rate threshold for the inhibition of thermal relaxation by moving dislocations, microphysical processes governed by dislocation motion could also explain the velocity threshold observed for dynamic weakening in experiments performed on different lithologies, including microgabbro, serpentinite, and Carrara marble as shown in Figure 1 [3,20]).

6. Prediction of V_w and T at the Asperity Scale Based on the Fast-Moving Dislocation Model

Assuming that the fast-moving dislocation model is applicable to fault rocks under seismic deformation conditions, it is possible to estimate the critical strain rate above which a thermal instability should occur. An estimate of the critical strain rate is given by setting the rate at which moving dislocations overcome the Peierls hill which is equal to the vibrational frequency of the dislocation f_d:

$$\dot{\gamma}^* = \frac{V}{h} = \frac{f_d \rho_{dis} b^2}{4} \tag{2}$$

where V is the applied velocity and h the thickness of the shear zone, with the assumption that only 25% of the total dislocations are moving under the applied stress field. The f_d in Equation (2) is [66]:

$$f_d = \frac{1}{dx}\sqrt{G/\{2\pi(1-\nu)\rho\}} \tag{3}$$

where dx is the dislocation length, G the shear modulus, ν the Poisson ratio, and ρ the mineral density. Using the properties for calcite (Table 1) and for a minimum dislocation length $dx = b$, where b is the Burgers vector, the expected values of f_d are $\sim 10^{11}$ s^{-1} in agreement with previous estimates [67]. Though there is not large variation in f_d between minerals, the dislocation density ρ_{dis} may vary considerably (e.g., [68,69]). The critical strain rate was thus determined from Equation (2) using a range of $\rho_{dis} = 10^{10}$–10^{14} m^{-2}, as shown in Figure 5 for calcite, serpentinite, and plagioclase (based on data in Table 1). From Equation (2), the critical strain rate is $\dot{\gamma}^* \sim 10^3$–10^5 s^{-1} in the case of calcite and, given a homogeneously distributed strain in a slipping zone of thickness h = [0.5–10] μm, $V^* = \dot{\gamma}^* h$ is approximatively in the range of 0.05–1 ms^{-1}. The lower estimate of V^* is compatible with the V_w measured in our experiments performed on calcite (~0.10 m/s) and with V_w resulting from experiments on other rocks, including silicate-bearing ones (e.g., Figure 1b; [5]). The temperature rise inside the

lattice can be estimated considering the work done by n dislocations moving at velocity v_{dis} under the shear stress σ [60]:

$$\Delta T \leqslant \begin{cases} \frac{k_s \, d^{\frac{1}{2}} v_{dis}}{16\pi K} ln\left(\frac{\Lambda}{\lambda}\right) & \text{for } \Lambda > \lambda \\ \frac{k_s \, d^{1/2} v_{dis}}{16\pi K}\left(\frac{\Lambda}{\lambda}\right)^{1/2} & \text{for } \Lambda \leqslant \lambda \end{cases} \quad (4)$$

where λ is the mean spacing of the dislocations, $\Lambda = \frac{2K}{\nu}$, $k_s = \frac{\pi \, G \, b}{4a}\sqrt{1/\lambda}$ is the microstructural shear stress intensity factor at the pile-up, d is the average grain size, $a = 2(1-v)(2-v)$ with v the Poisson's ratio, v_{dis} is the average velocity of dislocations inside the grain. It worth noting that $k_s \sqrt{d}$ in Equation (4) introduces the dependency of the critical shear stress on the grain size, as discussed in Section 7. Using Equation (4) with the thermal parameters listed in Table 1 for $\lambda = b$, $v = 0.3$ and $d = 0.3$ mm, ΔT can be of 10^4 °C already after only 1.5 mm of slip.

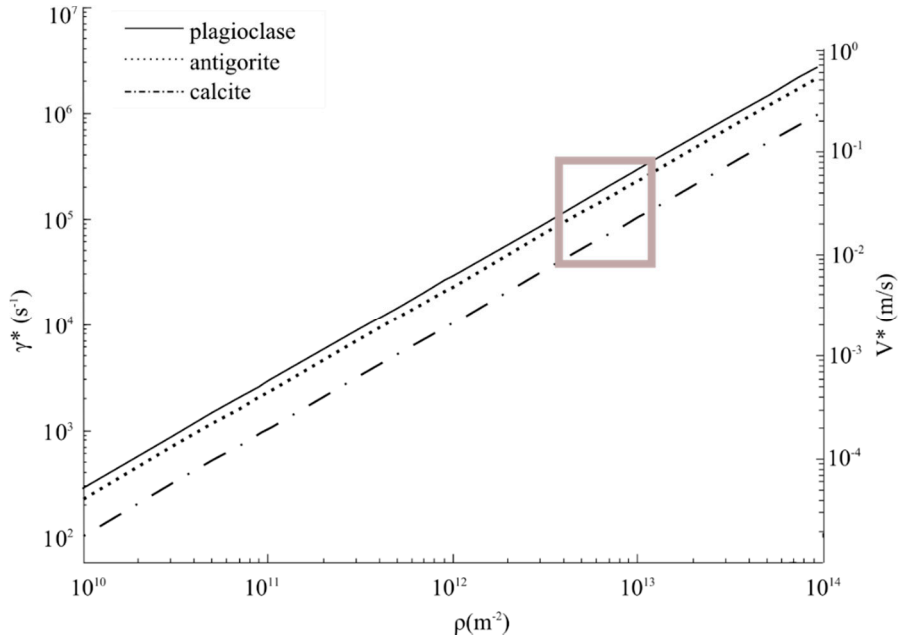

Figure 5. The fast moving dislocation model predicts the existence of a critical strain rate that determines the transition from ductile to brittle behavior. The critical strain rate depends on the dislocation velocity. The box indicates the region where dynamic weakening was observed in fault rocks deformed at seismic slip rates. The slip rate is calculated from the strain rate assuming a slipping zone deformation thickness of 0.5 μm, consistent with the microstructural observations in the case of experiments performed on Carrara marble, Figure 2a).

7. The Effect of Rock Texture on the Mechanism of Flash Heating

Generation and pile-up of mobile dislocations inside individual grains is controlled by the structure of the boundaries of the grains. Grain boundaries adjoin grains of different orientation so that more energy is required for a dislocation to pass into another grain. If dislocation motion is hindered, the onset of plasticity is inhibited resulting in an increase in yield strength. For this reason, pile-ups and brittle failure can initiate in a variety of ways depending on the combination of preferred planes where dislocations move (slip planes), grain size, and dislocation density.

The dislocation density and the grain size are interlaced by the size of a dislocation, because only a limited number of dislocations can fit within a submicron-sized crystal. The number of dislocations at the pile-up is relevant because dislocations generate a repulsive stress that reduces the energy barrier decreasing the amount of stress required to overcome the obstacle (the yield strength). Thus, the effect of a small grain size, which results in a low dislocation density, is to increase the yield strength at the obstacle. This behavior is ratified by the Hall-Petch relationship which states that dislocations

blocked at the strongest obstacle will increase the stress at the head of the pile-up till the yielding point (τ_p):

$$\tau_p = \tau_0 + k_y/\sqrt{d} \quad (5)$$

where τ_0 is the flow stress expected at a hypothetical infinite grain size d and k_y is a constant (i.e., the strengthening coefficient) derived empirically for each material, also known as the Hall-Petch parameter [70]. By rearranging Equation (1), the weakening temperature is:

$$T_w = T_f + \left(\frac{1}{\rho c\sqrt{k\pi}}\right)\tau_c\sqrt{d} * \sqrt{V_w} \quad (6)$$

where the rate of heat generation on the sliding interfaces is essentially the product of the sliding velocity times a measure of the shear strength. From the comparison of Equation (5) with Equation (6), and assuming $\tau_c = \tau_p - \tau_0$, it results that the heat production is a function of the grain size that impedes dislocation motion. If $V_w = V^* = \dot{\gamma}^* h$, Equation (6) can be interpreted as a measure of the heat produced by existing and newly generated dislocations moving under the applied stress field against the strongest obstacles.

Another important textural control on either hindering or facilitating dislocation motion is the orientation of the slip planes with respect to the applied stress field. In case of polycrystalline materials (i.e., microgabbro), the orientation of individual mineral grain boundaries can hinder dislocation motion whereas the existence of preferred crystallographic planes (i.e., cleavages in calcite) can help reducing the energy barrier at the pileup and in turn, the yield strength. The intervention of cleavage planes in the deformation of Carrara marble at short slips is shown by the river lines in Figure 6a [71,72] which are steps on the fractured surface between cleavage planes (Figure 6b). When a cleavage crack intersects a dislocation a step, a Burgers vector one unit high, is generated in the surface. Depending on the dislocation density and on the magnitude and orientation of the stress field the crack can split up into arrays of individual cracks as shown in inset of Figure 6b. The importance of cleavages and textural properties in controlling the brittle behavior of rocks was already recognized for dolomite [73], calcite [74], and feldspar [75]. The presence of exposed cleavage surfaces suggests that the initiation of weakening is also controlled by the amount of energy which can be converted into surface energy during brittle failure along cleavage planes.

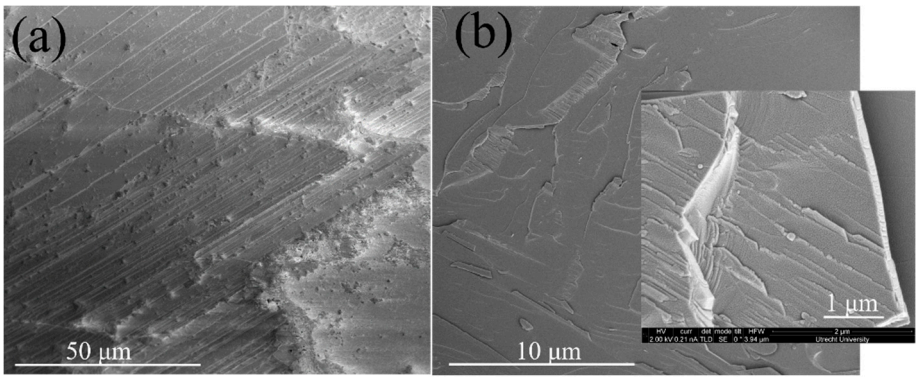

Figure 6. Exposed cleaved surfaces from SEM investigations on the slip surface of Carrara marble after 1.5 mm of slip. (**a**) River lines prevalent in the vicinity of the slip surface along cleavage, see also Figure 2b; (**b**) steps on the fracture surface between cleavage on parallel planes often indicated as resulting from intersection between cleavage fractures and moving dislocations [72]. The detail in the insert shows the splitting of a crack to form steps onto separate surfaces expanding past each other and then curving under the effect of mode II or mode III component in the stress field [71].

8. Implications for Earthquake Mechanics

The fast-moving dislocation model is in agreement with a number of natural and experimental observations of dynamic weakening of fault rock materials and may constitute the physical foundation of flash heating during frictional sliding. Though microstructural investigations are needed for feldspar- and serpentine-bearing rocks, we suggest the occurrence of a similar micro-mechanism operating at the onset of dynamic weakening during earthquakes in fault rocks.

Temperature-dependent deformation of polycrystalline materials can occur mainly by processes involving diffusional creep (stress-directed diffusion of vacancies, e.g., Coble creep, Nabarro-Herring creep, and pressure solution) and dislocation motion (dislocation creep and glide). The former tends to be the predominant deformation mode at lower stress level; both are typical deformation mechanisms of the viscous-plastic regime at crustal and mantle sub-seismic strain rates (10^{-14}–10^{-10} s^{-1}, e.g., [76–78] and references therein). Little is known about micromechanics associated with the high velocity side (10^{1}–10^{4} s^{-1} or seismic conditions) of the natural strain rate spectrum [79]. Our observations seem to suggest that the high velocity spectrum is likely dominated by brittle mechanisms over ductile mechanisms. The existence of a critical velocity for dynamic weakening and the fact that this critical velocity matches the prediction of a critical strain rate by a fast-moving dislocation model proposed here, seems to suggest that the transition to the brittle deformation mechanism is regulated by dislocation motion. In this view, dislocation motion gives continuity and generality to the frictional behavior of fault rock materials over the entire slip velocity spectrum from slow, sub-seismic to high seismic slip rates. The continuity is useful for earthquake modelling purposes where constitutive laws for frictional behavior need to account for the transition from the higher frictional resistance at sub-seismic slip rates towards the large dynamic weakening at seismic slip rates.

However, the strong relation between fast moving dislocations and fault weakening has another important consequence on earthquake mechanics. The deformation near a crack tip occurs over a region known as the plastic process zone (e.g., [78]). The process zone was described in terms of dislocation generation and motion at high strain rates [80]. It was found that the extent of the process zone decreased with increasing crack velocity indicating that the faster the material is stressed, the more brittle its behavior is. The dependency of the process zone on the microstructural evolution has two major implications: (1) part of the energy required to form new surface (and to propagate the rupture) comes from the strain energy stored within crystal dislocations and thus can be quantified; (2) the characteristic length scale of the constitutive laws in fracture mechanics depends on the loading rate, as a consequence of fast dislocation motion, and on the amount of energy stored within the crystal free for conversion in new surface energy. The balance between the available strain energy and the energy needed to propagate the slip (fracture energy) regulates seismic rupture on faults, controlling the earthquake magnitude and the amount of energy (seismic waves) radiated to the Earth's surface.

9. Conclusions

Earthquake mechanics is controlled by physical process taking place also at the nanoscale, though the underlying mechanisms are not well understood and may change over length scale and time (e.g., transition from flash melting to bulk melting). In this study we summarized recent results from high velocity friction experiments that simulate the passage of a rupture front on a point of a fault during earthquakes. We identify fast-moving dislocations as a possible micro-physical mechanism responsible for the high temperature rise associated with seismic slip and for the intense grain size reduction to the nanoscale in natural and experimental faults. We suggest that the fast-moving dislocation model is in agreement with flash-heating which was introduced in earthquake mechanics as a macro-physical description for fault weakening. Our investigations suggest that fast-moving dislocations and associated physico-chemical rock alterations may significantly contribute to fault weakening during earthquakes. However, further experiments and detailed microstructural investigations are needed.

Acknowledgments: This study was founded by the ERC CoG NOFEAR 614705 project (Giulio di Toro and Elena Spagnuolo) and supported through a Veni grant (863.13.006) awarded by the Netherlands Organization for Scientific Research, NWO (Oliver Plümper). We thank Piergiorgio Scarlato for laboratory support, Matthijs de Winter for technical support.

Author Contributions: Elena Spagnuolo wrote the paper; Elena Spagnuolo, Oliver Plümper, Giulio Di Toro, and Marie Violay contributed to the final version of the manuscript. Elena Spagnuolo and Oliver Plümper worked on concept development; Elena Spagnuolo, and Marie Violay conducted experiments; Oliver Plümper, and Andrea Cavallo did the microstructural analysis; all authors provided input into the interpretation of the microphysical mechanism.

Conflicts of Interest: The authors declare no competing financial interests.

References

1. Chang, J.C.; Lockner, D.A.; Reches, Z. Rapid acceleration leads to rapid weakening in earthquakes-like laboratory experiments. *Science* **2012**, *338*, 101–105. [CrossRef] [PubMed]
2. Rice, J.R. Heating and weakening of faults during earthquake slip. *J. Geophys. Res.* **2006**, *111*, B05311. [CrossRef]
3. Di Toro, G.; Han, R.; Hirose, T.; De Paola, N.; Nielsen, S.; Mizoguchi, K.; Ferri, F.; Cocco, M.; Shimamoto, T. Fault lubrication during earthquakes. *Nature* **2011**, *471*, 494–498. [CrossRef] [PubMed]
4. Tsustusmi, A.; Shimamoto, T. High-velocity frictional properties of gabbro. *Geophys. Res. Lett.* **1997**, *24*, 699–702. [CrossRef]
5. Goldsby, D.L.; Tullis, T.E. Flash heating leads to low frictional strength of crustal rocks at earthquake slip rates. *Science* **2011**, *334*, 216–218. [CrossRef] [PubMed]
6. Spagnuolo, E.; Nielsen, S.; Violay, M.; Di Toro, G. An empirically based steady state friction law and implications for fault stability. *Geophys. Res. Lett.* **2016**, *43*, 3263–3271. [CrossRef]
7. Rice, J.R. Flash heating at asperity contacts and rate-dependent friction. In *Eos Trans. AGU 80*, Proceedings of the AGU Fall Meeting F681, San Francisco, CA, USA, 13–17 December 1999.
8. Hirose, T.; Shimamoto, T. Growth of molten zone as a mechanism of slip weakening of simulated faults in gabbro during frictional melting. *J. Geophys. Res.* **2005**, *110*, B05202. [CrossRef]
9. Beeler, N.E.; Tullis, T.E.; Goldsby, D.L. Constitutive relationships and physical basis of fault strength due to flash heating. *J. Geophys. Res.* **2008**, *113*, B01401. [CrossRef]
10. Rempel, A.W.; Weaver, S.L. A model for flash weakening by asperity melting during high-speed earthquake slip. *J. Geophys. Res.* **2008**, *113*, B11308. [CrossRef]
11. Passelegue, F.X.; Goldsby, D.L.; Fabbri, O. The influence of ambient fault temperature on flash-heating phenomena. *Geophys. Res. Lett.* **2014**, *41*, 828–835. [CrossRef]
12. Proctor, B.P.; Mitchell, T.M.; Hirth, G.; Goldsby, D.; Zorzi, F.; Platt, J.D.; Di Toro, G. Dynamic weakening of serpentinite gouges and bare surfaces at seismic slip rates. *J. Geophys. Res.* **2014**, *119*, 8107–8131. [CrossRef] [PubMed]
13. Violay, M.; Nielsen, S.; Gilbert, B.; Spagnuolo, E.; Cavallo, A.; Azais, P.; Vinciguerra, S.; Di Toro, G. Effect of water on the frictional behavior of cohesive rocks during earthquakes. *Geology* **2014**, *42*, 27–30. [CrossRef]
14. Violay, M.; Di Toro, G.; Gibert, G.; Nielsen, S.; Spagnuolo, E.; Del Gaudio, P.; Azais, P.; Scarlato, P. Effect of glass on the frictional behavior of basalts at seismic slip rates. *Geophys. Res. Lett.* **2014**, *41*, 348–355. [CrossRef]
15. Di Toro, G.; Hirose, T.; Nielsen, S.; Pennacchioni, G.; Shimamoto, T. Natural and experimental evidence of melt lubrication of faults during earthquakes. *Science* **2006**, *311*, 647–649. [CrossRef] [PubMed]
16. Archard, J.F. The temperature of rubbing surfaces. *Wear* **1959**, *2*, 438–455. [CrossRef]
17. Tisato, N.; Di Toro, G.; De Rossi, N.; Quaresimin, M.; Candela, T. Experimental investigation of flash weakening in limestone. *J. Struct. Geol.* **2012**, *38*, 183–199. [CrossRef]
18. Violay, M.; Nielsen, S.; Spagnuolo, E.; Cinti, D.; Di Stefano, G.; Di Toro, G. Pore fluid in experimental calcite-bearing faults: Abrupt weakening and geochemical signature of co-seismic processes. *EPSL* **2013**, *361*, 74–84. [CrossRef]
19. Violay, M.; Di Toro, G.; Nielsen, S.; Spagnuolo, E.; Burg, J.P. Thermo-mechanical pressurization of experimental faults in cohesive rocks during seismic slip. *EPSL* **2015**, *429*, 1–10. [CrossRef]
20. Spagnuolo, E.; Plümper, O.; Violay, M.; Cavallo, A.; Di Toro, G. Fast-moving dislocations trigger flash weakening in carbonate-bearing faults during earthquakes. *Nat. Sci. Rep.* **2015**, *5*. [CrossRef] [PubMed]

21. Han, R.; Shimamoto, T.; Hirose, T.; Ree, J.-H.; Ando, J.I. Ultralow friction of carbonate faults caused by thermal decomposition. *Science* **2007**, *316*, 878–881. [CrossRef] [PubMed]
22. Han, R.; Hirose, T.; Shimamoto, T. Strong velocity weakening and powder lubrication of simulated carbonate faults at seismic slip rates. *J. Geophys. Res.* **2010**, *115*, B03412. [CrossRef]
23. De Paola, N.; Hirose, T.; Mitchell, T.; Di Toro, G.; Viti, C.; Shimamoto, T. Fault lubrication and earthquake propagation in thermally unstable rocks. *Geology* **2011**, *39*, 35–38. [CrossRef]
24. Green, H.W., II; Shi, F.; Bozhilov, K.; Xia, G.; Reches, Z. Phase transformation and nanometric flow cause extreme weakening during fault slip. *Nat. Geos.* **2015**, *8*, 484–489. [CrossRef]
25. Goldsby, D.L.; Tullis, T.E. Low frictional strength of quartz rocks at subseimic slip rates. *Geophys. Res. Lett.* **2002**, *29*, 25.
26. Di Toro, G.; Goldsby, D.L.; Tullis, T.E. Friction falls towards zero in quartz rich rock as slip velocity approaches seismic rates. *Nature* **2004**, *427*, 436–439. [CrossRef] [PubMed]
27. Philpotts, A.R. Origin of Pseudotachylites. *Am. J. Sci.* **1964**, *262*, 1008–1035. [CrossRef]
28. Sibson, R.H. Generation of pseudotachylyte by ancient seismic faulting. *Geopys. J. R. Astron. Soc.* **1975**, *43*, 775–794. [CrossRef]
29. Di Toro, G.; Pennacchioni, G. Superheated friction-induced melts in zoned pseudotachylytes within the Adamello tonalites (Italian Southern Alps). *J. Struct. Geol.* **2004**, *26*, 1783–1801. [CrossRef]
30. Collettini, C.; Viti, C.; Tesei, T.; Mollo, S. Thermal decomposition along natural carbonate faults during earthquakes. *Geology* **2013**, *421*, 927–930. [CrossRef]
31. Chen, J.; Yang, X.; Ma, S.; Spiers, J. Mass removal and clay mineral dehydration/rehydration in carbonate-rich surface exposures of the 2008 Wenchuan earthquake fault: Geochemical evidence and implications for fault zone evolution and coseismic slip. *J. Geophys. Res.* **2013**, *118*, 474–496. [CrossRef]
32. Smith, S.A.F.; Di Toro, G.; Kim, S.; Nielsen, S.; Billi, A.; Spiess, R. Coseismic recrystallization during shallow earthquake slip. *Geology* **2013**, *41*, 63–66. [CrossRef]
33. Kuo, L.W.; Song, S.R.; Suppe, J.; Yeh, E.C. Fault mirrors in seismically active fault zones: A fossil of small earthquakes at shallow depths. *Geophys. Res. Lett.* **2006**, *43*, 1950–1959. [CrossRef]
34. Stesky, R.M.; Brace, W.F.; Riley, D.K.; Robin, P.Y.; Robin, F. Friction in faulted rock at high temperature and pressures. *Tectonophys* **1974**, *23*, 177–203. [CrossRef]
35. Siman-Tov, S.; Aharonov, E.; Sagy, A.; Emmanuel, S. Nanograins from carbonate fault mirrors. *Geology* **2013**, *41*, 703–706. [CrossRef]
36. Fondriest, M.; Smith, S.A.F.; Candela, T.; Nielsen, S.; Mair, K.; Di Toro, G. Mirror-like faults and power dissipation during earthquakes. *Geology* **2013**, *41*, 1175–1178. [CrossRef]
37. Verberne, B.A.; Plümper, O.; de Winter, D.A.M.; Spiers, C.J. Superplastic nanofibrous slip zones control seismogenic fault friction. *Science* **2014**, *346*, 1342–1344. [CrossRef] [PubMed]
38. Kuo, L.W.; Li, H.; Smith, S.A.F.; Di Toro, G.; Suppe, J.; Song, S.R.; Nielsen, S.; Sheu, H.S.; Si, J. Gouge graphitization and dynamic fault weakening during the 2008 Mw 7.9 Wenchuan earthquake. *Geology* **2014**, *42*, 47–50.
39. Weertman, J.J. Continuum distribution of dislocations on faults with finite friction. *Bull. Seismol. Soc. Am.* **1964**, *54*, 1035–1058.
40. Fisher, D.S. Collective transport in random media: From Superconductors to Earthquakes. *Phys. Rep.* **1998**, *301*, 113–150. [CrossRef]
41. Poirier, J.P. *Creep of Crystals: High-Temperature Deformation Processes in Metals in Ceramics and Minerals*; Cambridge University Press: Cambridge, UK, 1985.
42. Holian, B.L.; Hammerberg, J.E.; Lomdahl, P.S. The birth of dislocations in shock waves and high-speed friction. *J. Comput. Aided Mater.* **2008**, *5*, 207–224. [CrossRef]
43. Di Toro, G.; Niemeijer, A.; Tripoli, A.; Nielsen, S.; Di Felice, F.; Scarlato, P.; Spada, G.; Alessandroni, A.; Romeo, G.; Di Stefano, G.; et al. From field geology to earthquake simulation: A new state-of-the-art tool to investigate rock friction during the seismic cycle (SHIVA). *Rend. Fis. Acc. Lincei* **2010**, *21*, S95–S114. [CrossRef]
44. Langenhorst, F. Shock metamorphism of some minerals: basic introduction and microstructural observations. *Bull. Czech Geol. Surv.* **2002**, *77*, 265–282.
45. Oganov, A.R. Structure, bonding, and mineralogy of carbon at extreme conditions. *Rev. Miner. Geochem.* **2013**, *75*, 47–77. [CrossRef]

46. Rice, J.R.; Cocco, M. Seismic fault rheology and earthquake dynamics. In *Tectonic Faults: Agents of Change on a Dynamic Earth*; Handy, M.R., Hirth, G., Hovius, N., Eds.; MIT Press: Cambridge, MA, USA, 2007; pp. 99–137.
47. Schön, J.H. Physical Properties of Rocks. In *Handbook of Petroleum Exploration and Production*; Cubitt, J., Ed.; Elsevier: Oxford, UK, 2011; Volume 8.
48. Melnikov, N.W.; Rshewski, W.W.; Prodotjakonov, M.M. *Spravocnik (Kadastr) Fiziceskich Svoištv Gornykh Porod*; Nedra: Moskow, Russia, 1975. (In Russian)
49. Cermak, V.; Rybach, L. Thermal properties. In *Landolt-Börnstein: Numerical Data and Functional Relationships in Science and Technology, New Series*; Hellwege, K.-H., Ed.; Springer-Verlag: Berlin, Germany, 1982; pp. 305–371.
50. Broz, M.E.; Cook, R.F.; Whitney, D.L. Microhardness, toughness, and modulus of Mohs scale minerals. *Am. Mineral.* **2006**, *91*, 135–142. [CrossRef]
51. Koholi, A.H.; Goldsby, D.L.; Hirth, G.; Tullis, T.E. Flash weakening in serpentinite at near-seismic slip rates. *J. Geophys. Res.* **2011**, *116*, B03202.
52. Goldsby, D.L.; Hirth, G. Frictional behavior of serpentine at high sliding velocity: Implications for seismic coupling at oceanic transform faults. In *Eos. Trans. AGU 87(52)*, Proceedings of the AGU Fall Meeting, T11C-0458, San Francisco, CA, USA, 11–15 December 2006.
53. Taylor, G.I. The Mechanism of Plastic Deformation of Crystals. Part I. Theoretical. *Proc. R. Soc. Lond. A* **1934**, *145*, 362–387. [CrossRef]
54. Gilman, J.J. Micromechanics of Flow in solids. In *McGraw-Hill Series in Materials Science and Engineering*, 1st ed.; McGraw-Hill: New York, NY, USA, 1969.
55. Weertman, J.; Weertman, J.R. *Elementary Dislocation Theory*; Oxford University Press: New York, NY, USA, 1992.
56. Hull, D.; Bacon, D.J. *Introduction to Dislocations*, 4th ed.; Butterworth-Heinemann, Elsevier Ltd.: New York, NY, USA, 2001.
57. Guyot, P.; Dorne, J.E. A critical review of the peierls mechanism. *Can. J. Phys* **1967**, *45*, 983–1016. [CrossRef]
58. De Hosson, J.T.; Roos, A.; Metselaar, E.D. Temperature rise due to fast-moving dislocations. *Philos. Mag. A* **2001**, *81*, 1099–1120. [CrossRef]
59. Roos, A.; de Hosson, J.T.M.; der Giessen, E.V. High-speed dislocations in high strain-rate deformations. *Comput. Mater. Sci.* **2001**, *20*, 19–27. [CrossRef]
60. Armstrong, R.W.; Elban, W.L. Temperature rise at a dislocation pile-up breakthrough. *Mater. Sci. Eng.* **1989**, *122*, L1-3. [CrossRef]
61. Armstrong, R.W. Dislocation mechanics aspects of energetic material composites. *Rev. Adv. Mater. Sci.* **2009**, *19*, 13–40.
62. Armstrong, R.W. Dislocation mechanisms for shock-induced hot spots. *J. Phys. IV France* **1995**, *5*, C4.89–C4.102. [CrossRef]
63. Cleveringa, H.; der Giessen, E.V.; Needleman, A. A discrete dislocation analysis of mode I crack growth. *J. Mech. Phys. Solids* **2000**, *48*, 1133–1157. [CrossRef]
64. Duvall, G.E.; Fowles, G.R. Chapter 9: Shock waves. In *High Pressure Physics and Chemistry*; Bradley, R.S., Ed.; Academic Press: New York, NY, USA, 1963.
65. Melosh, H.J. *Impact Cratering: A geologic Process*; Oxford University Press: New York, NY, USA, 1989; p. 245.
66. Kratochvil, J.J.; Kroupa, F. Internal vibrations of edge dislocation dipoles. *Res. Lett. Mater. Sci.* **2008**, *2008*, 907895. [CrossRef]
67. Kocks, U.F.; Argon, A.S.; Ashby, M.F. Thermodynamics and kinetics of slip. *Prog. Mater. Sci.* **1974**, *19*, 292.
68. Gilman, J.J., II. Cleavage, ductility, and tenacity in crystals. In *Fracture*, Proceedings of International Conference on Atomic Mechanisms of Fracture, Swampscott, MA, USA, 12–16 April 1959; Wiley: Hoboken, NJ, USA, 1959; pp. 193–222.
69. De Bresser, J.H.P. Steady state dislocation densities in experimentally deformed calcite materials: Single crystals versus polycrystals. *J. Geophys. Res.* **1996**, *101*, 22,189–22,201. [CrossRef]
70. Hansen, N. Hall-Petch relation and boundary strengthening. *Scr. Mater.* **2004**, *51*, 801–806. [CrossRef]
71. Hull, D. The effect of mixed mode I/III on crack evolution in brittle solids. *Int. J. Fract.* **1995**, *70*, 59–79. [CrossRef]
72. Abbashian, R.; Abbaschian, L.; Reed-Hill, R.R. *Physical Metallurgy Principles*, 4th ed.; Cengage Learning: Stamford, CT, USA, 2008; p. 693.

73. Austin, N.J.; Kennedy, L.A.; Logan, J.M.; Rodway, R. Textural controls on the brittle deformation of dolomite: The transition from brittle faulting to cataclastic flow. *Geol. Soc. Lond. Spec. Publ.* **2005**, *243*, 51–66. [CrossRef]
74. Fusseis, F.; Handy, M. Micromechanisms of shear zone propagation at the brittle-viscous transition. *J. Struct. Geol.* **2008**, *30*, 1242–1253. [CrossRef]
75. Tullis, J.; Yund, R.A. Transition from cataclastic flow to dislocation creep of feldspar: Mechanisms and microstructures. *Geology* **1987**, *15*, 606–609. [CrossRef]
76. Ashby, M. A first report on deformation mechanism maps. *Acta Metall.* **1972**, *20*, 887–897.
77. Rutter, E.H. The kinetics of deformation by pressure solution. *Phil. Trans. R. Soc. Lond. A* **1976**, *283*, 203–213. [CrossRef]
78. Scholz, C.H. *The Mechanics of Earthquakes and Faulting*, 2nd ed.; Cambridge University Press: Cambridge, UK, 2002; p. 471.
79. De Paola, N.; Holdsworth, R.E.; Viti, C.; Collettini, C.; Bullock, R. Can grain size sensitive flow lubricate faults during the initial stages of earthquake propagation? *Earth Planet. Sci. Lett.* **2015**, *43*, 48–58. [CrossRef]
80. Tetelman, A.S. *Fracture in Solids*; Drucker, D.C., Gilman, J.J., Eds.; Interscience: New York, NY, USA, 1963; p. 461.